COMPUTATIONAL MULTISCALE ANALYSIS FOR INTERLAMINAR REINFORCEMENT OF COMPOSITE LAMINATES WITH RADIALLY GROWN CARBON NANOTUBE ARCHITECTURE

Karthik Rajan Venkatesan and Aditi Chattopadhyay

Arizona State University
Tempe, Arizona, USA
*Corresponding Author: aditi@asu.edu

ABSTRACT

A multiscale modeling framework that integrates nanoscale-informed constitutive models is employed to predict the interlaminar and intralaminar enhancement in composite laminates with radially-grown carbon nanotube (CNT) architecture. The nanoscale-informed constitutive models are implemented using the high-fidelity generalized method of cells (HFGMC) technique accounting for the material constituents and imperfect interfaces at the microscale. The micromechanical model is then coupled with the finite element model of a composite laminate specimen at the macroscale. The developed computational modeling framework is exercised to predict the initiation and steady-state toughness of mode I fracture composite samples. The results obtained from the simulations are correlated to the available experimental data collected from the literature. Conclusions are presented comparing the model response of traditional fiber reinforced polymer (FRP) composite laminates and composites with radially-grown CNT architecture.

1. INTRODUCTION

Due to their exceptional multifunctional properties, the use of carbon nanotubes (CNTs) as nanoscale reinforcements has been widely explored to improve the mechanical properties of low weight structures with potential applications in aerospace and civil technologies [1-3]. A common use for CNTs is a reinforcement of traditional fiber reinforced polymer (FRP) composites [4,5]. In traditional FRP, the interface between the plies is well known to be a 'weak link' in laminated composites, which requires significant reinforcement along the out-of-plane direction. Several approaches for CNT reinforcement are explored to strengthen both the interlaminar and intralaminar regions, with much of the work involving CNTs dispersed into the polymer matrix region [6-9]. However, due to substantial issues in processing and controlling CNT alignments, only marginal improvements in properties are observed.

Grafting or growing CNTs on the surface of fibers (fuzzy fibers) offers some advantages over other approaches [10,11]. The introduction of CNTs in this manner provides a higher level of control over CNT length and orientation [12]. Radially-grown CNT fuzzy fibers show high potential for mechanical reinforcement and offer improved load transfer between the fibers/matrix interface and increased interfacial shear strength (IFSS) [13,14]. Therefore, the use of fuzzy fiber architecture offers enhanced interlaminar and intralaminar properties over other approaches [15,16,17].

The improvement in properties is mainly attributed to the presence of radially-grown CNTs creating an additional layer of stiffness around the fiber and spanning interply matrix regions [11,18]. For adequate assessment of these performance gains, one would require detailed modeling on the behavior of CNT reinforced fiber/matrix interphase, matrix, and interlaminar region. Several models have been proposed by various authors to determine the mechanical properties of fuzzy fiber reinforced composite using effective properties approaches and multiscale modeling techniques [19-22]. The effect of CNT bridging in the interlaminar region was also modeled using a closed-form analytical solution to predict the magnitude of toughness enhancement due to the fuzzy fiber reinforcement [23]. However, these methods are often not adequate as they fail to capture the complex interactions between constituent interface/interphases across multiple length scales.

In this work, a multiscale modeling framework that integrates the nanoscale model of the various constituent material phases is presented, to investigate the enhancement in out-of-plane properties in traditional FRP composite with fuzzy fiber architecture. The CNT enhanced fiber/matrix interface at the sub-microscale is modeled using nanoscale properties and physical damage evolution law that uses the fundamental bond breakage information from molecular dynamics simulations. A high-fidelity generalized method of cells approach is employed to model the fuzzy fiber composite microstructure. The micromechanical model is integrated within a finite element model of a mode I composite laminate specimen, and the composite fabric plies properties derived from a two-step homogenization procedure. A traction-separation law based on the atomistic bond dissociation information is presented to model the epoxy adhesive layer in the interlaminar region. The multiscale framework is then employed to predict load-displacement response and fracture toughness from the mode I virtual simulations. The predicted values are correlated to available experiment results from the literature.

2. MULTISCALE MODELING FRAMEWORK

As shown in Figure 1, a bottom-up multiscale modeling framework is proposed to take into consideration the complex mechanisms of deformation at various length scales for composites with carbon nanotube architecture. In the bottom level of the modeling approach, nanoscale simulations are used to capture the complex interactions between constituent phases in the composite. The nanoscale properties are used to develop sub-microscale continuum models to inform the properties of the constituents at the microscale. Computational homogenization of a Repeating Unit Cell (RUC) of the microstructure is used to predict the lamina's properties from the properties of the constituents such as the polymer matrix, the fiber and the CNT reinforced interphase region. At the mesoscale, unit cells with plain weave geometry use the homogenized results of the micromechanical models as constitutive models for each lamina. At the macroscale level, the Mode I composite laminate virtual tests are carried out using three-dimensional elements whose constitutive properties are provided by the mesoscale model. The elastic properties of the laminate are readily obtained using the homogenization procedure while the onset of damage is provided by the constitutive material models at the sub-microscale.

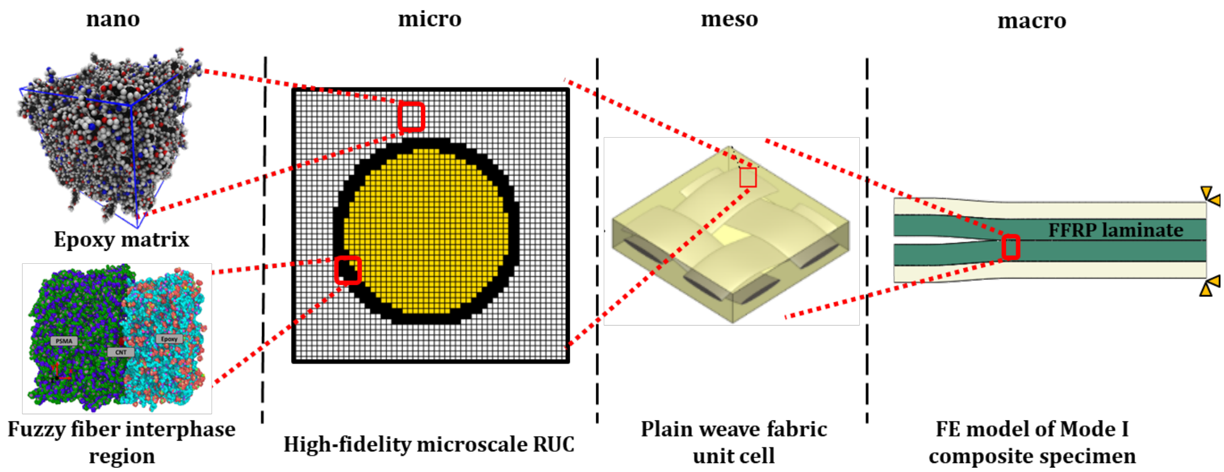

Figure 1. Nano-macro multiscale modeling scheme

2.1 Nanoscale model

In our previous studies, the nanoscale model of the neat epoxy matrix and radially-grown CNT/fiber (fuzzy fiber)/epoxy interphase region was investigated using molecular dynamics simulations. A difunctional resin, bisphenol-F epoxy resin was used in the neat polymer unit cell. The unit cell was cured based on a stochastic cutoff distance approach [24]. The effect of crosslinking degree in the epoxy matrix on the overall elastic properties such as Young's modulus, bulk, and shear moduli are discussed in [25]. Similarly, the effect of the addition of radially-grown CNTs in the fiber/matrix interface was captured using the nanoscale interphase unit cell [26]. The interphase unit cell consists of radially-grown single wall CNTs, epoxy resin, carbon fiber surface and a polymeric functional coating on the fiber surface. Figure 1 illustrates a cured epoxy system and radially-grown CNT/fiber/epoxy interphase unit cell in the nanoscale column.

At the nanoscale, the damage initiation phenomenon is primarily driven by the polymer mechanics arising from a fundamental level due to stretching and dissociation of covalent bonds in the system. The presence of CNTs, particularly in the fiber/matrix interface creates a complex stress state due to the non-bonded interactions with the surrounding polymer. The nanoscale models utilize a bond-order based forcefield, also known as a reactive force field, to simulate the covalent bond elongation and breakage. Virtual deformation tests were performed to capture the elastic characteristics and the complex damage process. The variation of nanoscale bond energy between the deformed and undeformed state is used to quantify bond dissociation energy (BDE). The change of BDE as a function of applied strain is related to damage precursors at higher length scales. Consequently, the elastic properties and corresponding BDE variation with strain are used to define material constitutive behavior at the continuum level. Further details on the model setup and MD system and simulation methodology can be found in references: [26].

2.2 Micromechanical model

2.2.1 Constitutive law

The material properties for the fibers are modeled as transversely isotropic solids with linear elastic constitutive law. The epoxy matrix of the composite material is modeled as a linear elastic isotropic solid with elastic and nonlinear properties obtained using a previously developed constitutive model based on variation in the polymer crosslinking degree. This enables the unit cell to capture the damage behavior of the epoxy matrix which utilizes damage evolution equation developed to simulate the BDE response of the system at the nanoscale. The constitutive model was developed based on the continuum damage mechanics (CDM) approach, with damage evolution equations formulated as a functional form of nanoscale simulation results of the BDE variation under applied strain. The continuum equation for the damage evolution for varying crosslinking degree reproduces the complex nanoscale damage process and is given as

$$\dot{D} = \frac{\dot{\lambda}}{2}\left[\operatorname{sgn}(x)\frac{-(1-\eta)|x| - |x|}{2(1-\eta)|x| + (1-\eta) - 1} + 1\right] \qquad [1]$$

$$x = 2\left(\frac{Y}{Y_0}\right)^{\frac{1}{2(1-\eta)}} - 1 \qquad [2]$$

where λ is the viscoplastic multiplier, η is the crosslinking degree, Y is the elastic energy and Y_0 is the minimum energy required to initiate damage in the material. Further details on the continuum formulations and derivations can be found in references [27].

The fuzzy fiber interphase region is modeled as linear elastic orthotropic material with elastic properties obtained using tensile and shear virtual deformation simulations of the nanoscale interphase model. The CDM framework was used to develop the constitutive material model for radially-grown CNT fuzzy fiber interphase region. In our previous study, we focused on capturing the effect of CNT areal density (number of CNTs per nm^2) on the elastic and damage initiation characteristics of the critical interphase region. Despite the orthotropic nature of the interphase region, nanoscale investigations revealed that failure of the interphase under deformation transverse to the CNT growth was more pronounced and dominant compared to the direction along the CNT growth and along the fiber [26]. Therefore, the damage was modeled along the direction transverse to the CNT growth and the nanoscale BDE information was used to develop the equation for damage evolution for varying CNT areal density, as shown in Eq. (3a) and (3b).

$$\dot{D_s} = \frac{\dot{\lambda}}{2}\left[\frac{(1+\alpha) - D_s\rho^{\eta}}{\rho^{\eta}}\right]Y^{\xi} \qquad [3a]$$

$$\xi = \alpha\rho^{\eta} \qquad [3b]$$

where ρ is the CNT areal density, α is a phenomenological constant and η is the rate of damage growth calibrated to reproduce nanoscale BDE response. Further details on the continuum formulations for fuzzy fiber interphase constitutive model can be found in [28].

2.2.2 Model set-up

To capture the role of radially-grown CNT/fuzzy fiber interphase on the intralaminar mechanical behavior, the HFGMC based micromechanics theory is established. With HFGMC, the microscale unit cell is defined by a continuous long fiber inclusion in a polymer matrix. The unit cell is discretized into several subcells. The critical interphase region is modeled as interphase subcells of uniform thickness adjacent to the fiber subcells as illustrated in Figure 2(a). Additionally, the interphase subcells are modeled as cylindrically orthotropic, and the material properties are transformed with respect to the angle formed by the in-plane axis of the nanoscale unit cell along the CNT growth direction to the out-of-plane axis along the fiber direction. The material input parameters are summarized in Table 1 and Table 2. The orthotropic elastic properties obtained from nanoscale simulations are incorporated into the micromechanical model using the strain transformation matrix and is expressed as

$$\bar{C}_{int} = T_{\epsilon} C_{int} T_{\epsilon}^{T} \quad [4]$$

Table 1. Elastic material properties of the matrix, fiber and CNT reinforced interphase

Material	E_1 (GPa)	E_2 (GPa)	E_3 (GPa)	G_{12} (GPa)	G_{13} (GPa)	G_{23} (GPa)
Fiber	294	18.5	18.5	7.1	7.1	25
Epoxy	1.8	1.8	1.8	0.64	0.63	0.64
Interphase	17.32	15.39	27.61	2.35	4.58	3.16

Table 2. Input material properties for damage model of matrix and CNT reinforced interphase

Material	Parameters
Epoxy	$Y_0 = 0.12,\ \eta = 0.19$
Interphase	$\alpha = 0.20,\ \eta = 0.042$

The CNT volume fraction of the radially-grown architecture is given by a simple geometric relationship based on a unit cell with a single fiber, and CNT reinforced interphase region and is given as

$$V_{cnt}(\%) = \frac{\rho \pi d_{cnt}^2 t_{int}}{D} V_f \times 100 \quad [5]$$

where D and V_f are the diameter and volume fraction of the fiber, d_{cnt} is the diameter of radially-grown CNTs, t_{int} characterizes the thickness of the interphase region, and ρ is the CNT areal density at the sub-microscale. It is important to note that the interphase thickness is assumed to adequately capture the experimentally observed reinforcing effect and is primarily dictated by a sub-microscale scaling factor estimated from the nanoscale model in Ref. [26]. The scaling factor used in the present microscale model based on the nanoscale unit cell is estimated to be ~ 0.33.

2.3 Mesoscale model

A two-step homogenization procedure is utilized to predict the elastic material properties of plain weave fabric plies with radially-grown CNT fuzzy fiber. The first step fundamentally idealizes the microscale fiber/matrix system. The HFGMC based unit cell described in the previous section is used to obtain the stiffness matrix of the homogenized composite microstructure. The second step is employed to homogenize the plain weave geometry into a single ply with orthotropic elastic properties. Therefore, a secondary HFGMC mesh is generated, which, for an ideal case, represents the checkboard geometry of a composite plain weave ply.

A plain weave unit cell is assumed to consist of two forms of subcells that are repeated to form the checkboard geometry. One subcell represents unidirectional fuzzy fibers running in the primary direction, and the adjacent subcell represents fuzzy fibers running in the transverse direction. The homogenized elastic properties of the subcells constituting fibers in the primary direction are obtained from the first step HFGMC procedure. The obtained stiffness matrix is then rotated 90 degrees to inform the properties of the subcells with fibers running in the transverse direction. Additionally, the homogenized plain weave unit cell also captures intralaminar damage and failure due to damage in the microscale unit cell. A schematic representation of the two-step homogenization procedure, and the relationship between microscale and weave fabric coordinate system is shown in Figure 2(b).

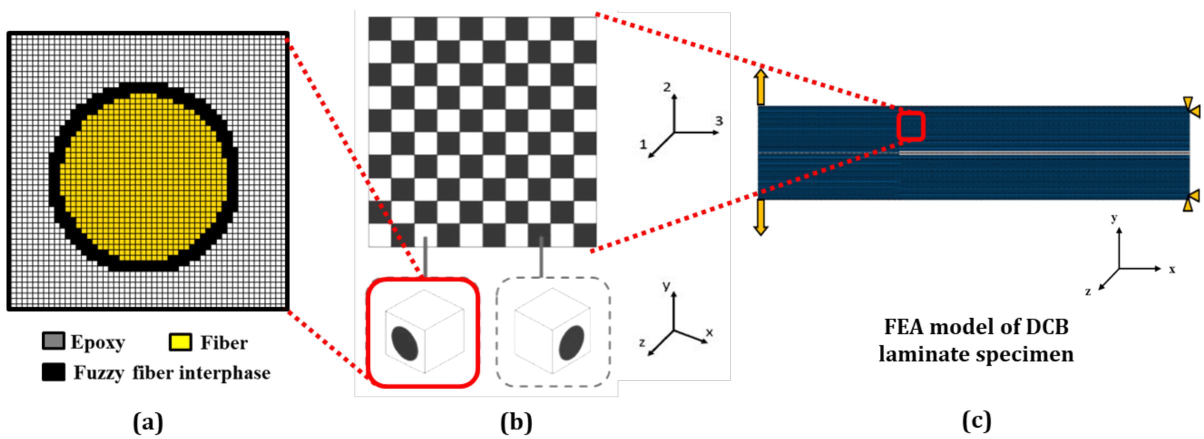

Figure 2. Homogenization procedure for composite plain weave fuzzy fabric properties: (a) microscale RUC; (b) plain weave checkboard pattern unit cell; (c) FFRP composite laminate

2.4 Macroscale model

2.4.1 Model set-up

At the macroscale, the fiber-reinforced composite laminates are considered with the dimensions of 152.4 mm x 20 mm and a total of 8 plies with a thickness of 1 mm for each ply. The Double Cantilever Beam (DCB) test is commonly used to estimate the mode I interlaminar fracture toughness in a composite laminate. Therefore, to facilitate DCB laminates, an initial delamination crack of 50 mm length and thickness t = 0.025 mm is placed between the middle plies on the last 50 mm on one end of the composite laminate. An epoxy adhesive layer of the same thickness is placed on the remaining length of the laminate. The mode I composite laminate specimen is created in Abaqus/Explicit, as shown in Figure 3. The interlaminar properties between the plies with the adhesive layer are modeled using cohesive elements of finite thickness. The material properties for the laminates are informed using the mesoscale model. The cohesive behavior of the adhesive layer is modeled using the nano-informed traction-separation model, discussed in the next subsection.

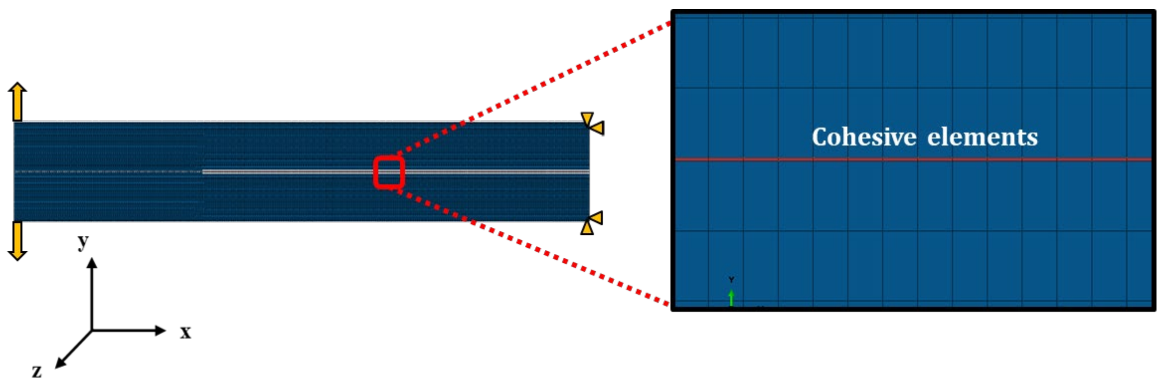

Figure 3. Schematic view of the macroscale finite element model showing, DCB specimen, and interlaminar cohesive interface

The laminate geometry meshes with an edge size of 0.25 mm x 0.5 mm within the *x-y* plane. An enhanced viscous-based hourglass control is employed to suppress spurious energy modes, and mass scaling is used to achieve the critical stable time increment. The loading and boundary conditions applied to the macroscale composite model is illustrated in Figure 3. The right edges are constrained in all three directions. A reference point is introduced in the top and bottom of the left end and is kinematically tied to the nodes on the top and bottom edges using TIE constraints. A displacement load is applied to the reference points, and the resulting reaction forces are readily obtained. The developed modeling framework is used to predict load-displacement response for traditional fiber reinforced composites and composites with fuzzy fiber architecture, to investigate the role of radially-grown CNTs on the onset and propagation of delamination.

2.4.2 Cohesive zone model

The adhesive layer is substantially the resin region that exists between adjacent plies of the composite laminate. Consequently, the element based cohesive behavior is used to capture the interply delamination using the atomistically informed continuum model for the epoxy matrix. The cohesive zone model assumes that the degradation in load transfer between the two plies is a progressive event governed by a cohesive material law based on a quadratic stress criterion. The continuum formulations are utilized to model the traction-separation response of the epoxy matrix under different modes of loading. The continuum stresses for an isotropic material are given by

$$\sigma_i = \frac{\epsilon_i}{{\epsilon^c}_i}\sigma_{max}(1 - \boldsymbol{D}_i) \quad [6]$$

where ϵ_i is the strain along the loading direction, σ_i as the corresponding stress, σ_{max} as the maximum stress or yield strength, and ${\epsilon^c}_i$ as the critical strain. The continuum damage variable D_i is computed using the atomistically-informed damage equation for varying crosslinking degree, shown in Eq. [1]. At the continuum level, if the adhesive material is represented by a very thin layer of finite thickness t, and assuming uniform strain along the thickness, the elastic stiffness K, displacement δ are expressed as

$$\{K_{nn}\ K_{ss}\ K_{tt}\} = \frac{1}{t}\cdot\{E_{11}\ G_{12}\ G_{13}\} \quad [7]$$

$$\{\delta_{nn}\ \delta_{ss}\ \delta_{tt}\} = t\ \cdot\{\epsilon_{11}\ \epsilon_{12}\ \epsilon_{13}\} \quad [8]$$

where *nn, ss, tt* corresponds to normal, first shear and second shear direction. The specific material properties for the cohesive law are shown in Table 3.

Table 3. Input material properties for cohesive interface elements

	$\boldsymbol{K_{nn}}$ (MPa/mm)	$\boldsymbol{K_{ss,tt}}$ (MPa/mm)	$\boldsymbol{T_{max}}$ (MPa)	$\boldsymbol{{\delta^c}_{nn}}$ (mm)	$\boldsymbol{{\delta^c}_{ss,tt}}$ (mm)
Cohesive Parameters	72000	25600	63.45	0.00087	0.0025

Equation (7) is then modified to obtain the traction-separation response of the cohesive adhesive layer as

$$T_i = \frac{\delta_i}{{\delta^c}_i}T_{max}(1 - \boldsymbol{D}_i) \quad [9]$$

Figure 4 shows the normalized traction-separation response of the cohesive adhesive layer of the epoxy matrix with a 20 % crosslinking degree. From the simulated traction-separation response, the corresponding damage variables for the respective displacements are directly implemented in ABAQUS using the tabular capability as a function of relative displacement.

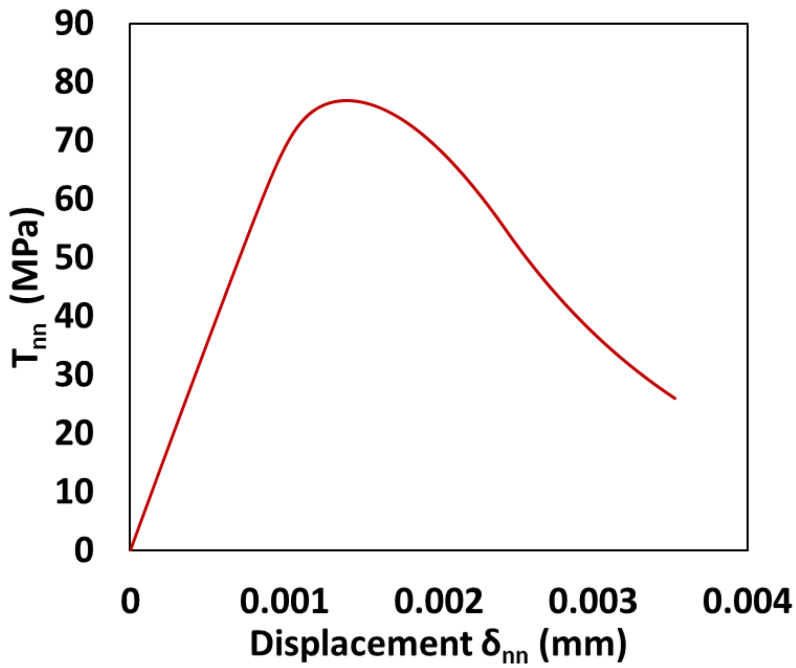

Figure 4. Normalized traction-separation relationship in the normal direction corresponding to the cohesive model material properties in Table 3.

3. RESULTS AND DISCUSSION

To validate the methodology developed in this paper, the results for Mode I DCB experiments presented in [11, 23] are used. In Ref. [11], fuzzy fiber reinforced polymer composite laminates were manufactured with CNTs radially-grown to a height of 6 μm on microfiber surface of diameter D = 15 μm. The radially-grown CNTs were sufficiently long to span the interply matrix regions and thus formed a uniform growth pattern around the fiber. The baseline and FFRP laminates were manufactured 8 plies thick with the unmodified difunctional resin based marine epoxy. The microfiber volume fraction of composite laminates was 35-43 % for baseline (no CNTs) and 44-50 % for short radially-grown CNTs, with resulting CNT weight fraction in the laminate at 0.5 %, respectively. The multiscale model, generated with these properties, is integrated within the finite element model of Mode I DCB composite specimen.

The radially-grown CNTs enhances the resin rich regions between plies combined with intralaminar reinforcement within each ply. Hence, the fracture process is different from that of a baseline composite. However, in the present model, a single traction-separation model for the interlaminar region with neat resin is used for both models. Consequently, only the isolated effects of the intralaminar reinforcement on toughness enhancement are captured in the present model. It should also be noted that an areal density of ~200 CNTs per μm^2 and a fuzzy fiber interphase thickens of ~ 6 μm is chosen to model ~ 0.5 % weight fraction of CNT. The effect of fuzzy fiber architecture is investigated by comparing the load-displacement response obtained from the Mode I DCB simulations for the baseline and FFRP model. The load-displacement curve is calculated by extracting the reaction forces and applied displacement load associated with the two reference points on the top and bottom end. The reference points emulate the function of load hinges in the Mode I DCB test. The FE computed load-displacement response is shown in Figure 5 in terms of reaction force P and the relative displacement δ.

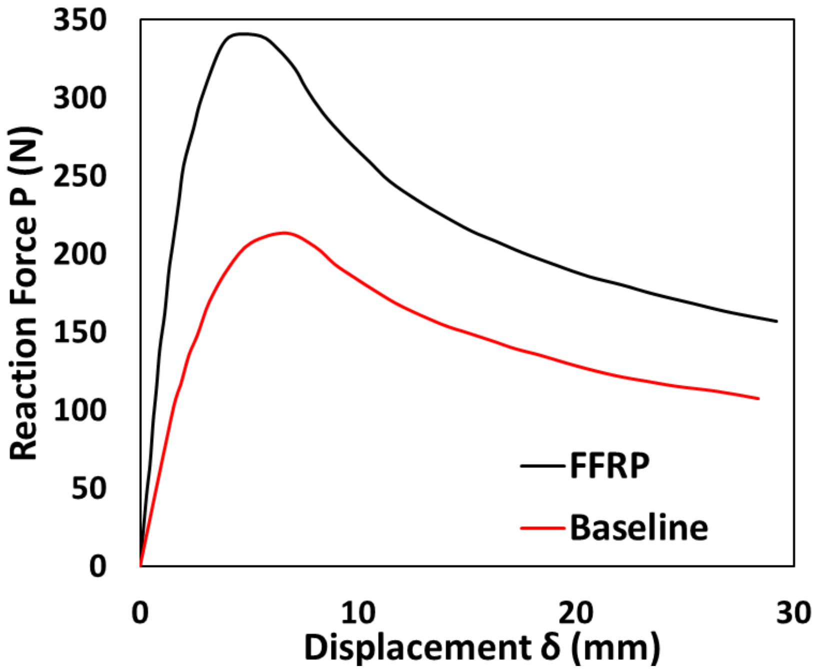

Figure 5. Multiscale model predictions for the Mode I DCB load-displacement response of radially-grown CNT (0.5 % weight fraction) and baseline fiber reinforced composite

The increased slope of the load-displacement curve in Figure 5 is attributed to the presence of radially-grown CNTs on fiber, which enhances the intralaminar region in the direction transverse to the plain weave fabric. Consequently, the multiscale model predicts a 59 % increase in the peak load. Mode I toughness is characterized by resistance curves (R-curves), which indicate the initiation and steady-state toughness during the delamination process in the composite laminate specimen. Under the assumption of mechanical and geometric linearity, the energy release rate for the Mode I composite specimen [29] is given by

$$G = \frac{P^2}{2B}\frac{\partial C}{\partial a}, \qquad C = \delta \,/\, P \qquad [10]$$

where P, is the reaction load, δ is the applied opening displacement, B is the laminate's width, C is the compliance, and a is the delamination crack length. The Compliance Calibration (CC) method [30] is used, where the compliance obtained from the FE simulation is fitted using the least square methods.

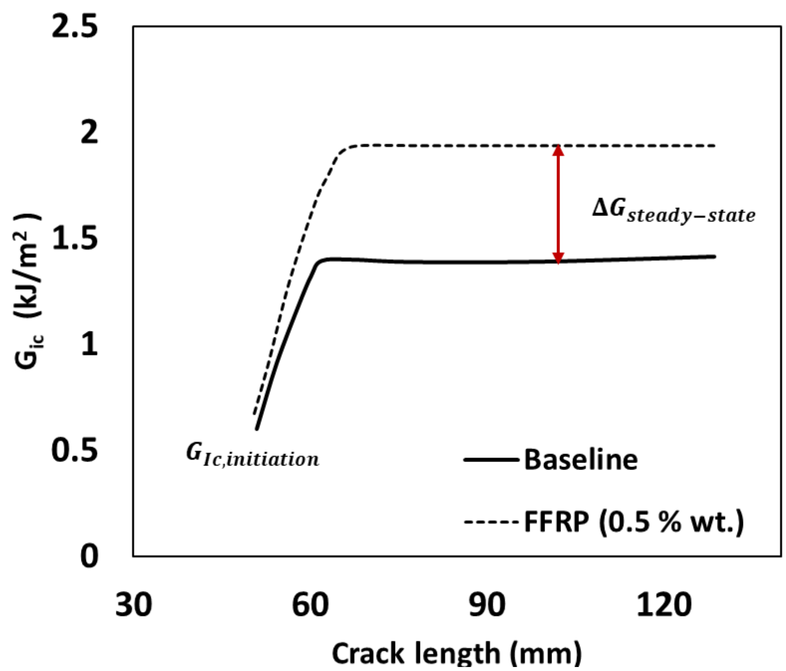

Figure 6. Model predictions for the Mode I resistance curve of radially-grown CNT and baseline fiber reinforced composite calculated using the CC method.

Figure 6 shows the representative R-curves obtained from the simulation for baseline and FFRP composite laminates. A comparison of the predicted energy release rate at initiation shows that the initiation toughness for FFRP composite increases ~ 11.4 % above the baseline composite, and the steady-state toughness improves by 42.9 % compared to the baseline composite. The fiber properties, volume fraction and the cohesive interface strength properties are adjusted for baseline composite model to get a close match with the experiments. Using the adjusted parameters, the model predictions for initiation fracture toughness in FFRP composites are well within the range obtained from experiments. However, the model predictions show only a 42.9 % in steady state toughness compared to the ~89 % improvement observed in the experimental results presented in [11]. A summary of the data from the multiscale model and obtained experimental data is presented in Table 4.

Table 4. Comparison of Mode I fracture toughness between experiments and multiscale model

Material	Multiscale model		Experimental data	
	$G_{Ic, initiation}$ (kJ/m^2)	$G_{Ic, steady-state}$ (kJ/m^2)	$G_{Ic, initiation}$ (kJ/m^2)	$G_{Ic, steady-state}$ (kJ/m^2)
Baseline (no CNTs)	0.6	1.35	0.57 ± 0.26	1.19 ± 0.09
FFRP (0.5 % wt.)	0.67 {11 % ↑}	1.93 {42 % ↑}	0.74 ± 0.33 {33 % ↑}	2.25 ± 0.19 {89 % ↑}

The mismatch in the steady-state toughness between model and experiments could be due to an underestimation around the peak load, which may be attributed to additional changes in the growth zone bridging from transient to a steady propagation in fuzzy fiber architecture. The authors hypothesize that this could be because of the effect of CNT bridging in the interlaminar region, which is not captured in the present traction-separation model. However, it is noteworthy to mention that the developed framework can predict enhancement in interlaminar Mode I toughness merely due to intralaminar reinforcement of the fiber/matrix interface at the nano and sub-microscale. Further investigation on modeling the interlaminar region is needed to understand the underlying physical mechanisms fully and adequately capture the effect of CNT bridging in fuzzy fiber architecture.

4. CONCLUSIONS

This paper presents an atomistically-informed multiscale modeling framework, bridging nanoscale information to macroscale, which enables the prediction of interlaminar and intralaminar enhancements in fiber reinforced composite laminates with radially-grown carbon nanotube (CNT) architecture. The developed framework utilized material properties and damage models for the radially-grown CNT/fiber/matrix interphase and a neat polymer resin, modeled using molecular dynamics simulations. Previously determined nanoscale properties were used to model the effect of CNT enhanced fiber/matrix interphase region at the nanoscale. An existing nano-informed damage model for the polymer was used to model the traction-separation response of the resin in the interlaminar region. The microscale fiber/matrix system was modeled using a high-fidelity generalized method of cells micromechanics approach. The elastic properties of the plain weave fuzzy fiber plies were modeled using a two-step homogenization process of the microscale unit cell. The macroscale geometry of a Mode I composite laminate specimen was modeled using finite elements.

The load-displacement response obtained from Mode I virtual simulations showed improved stiffness and peak load in case of fuzzy fiber composite architecture. The overall effect of radially-grown CNTs on the delamination resistance was further investigated by comparing the resistance curves (R-curves) with traditional FRP composites. The addition of radially-grown CNTs on fiber was shown to improve the initiation and steady-state Mode I fracture toughness of fiber reinforced laminated composites by 11 % and 48 %, respectively. However, the value of steady-state toughness for fuzzy fiber composite was underestimated compared to experiments in the literature. Future investigation will include explicit modeling of the effect of CNT bridging in the interlaminar region to improve the accuracy of the predicted results.

Acknowledgments

This research is supported by the Office of Naval Research (ONR), Grant number: N00014-17-1-2037. The program manager is Mr. William Nickerson. The authors also acknowledge Dr. Anisur Rahman, a technical liaison for this research and the DoD ERDC Supercomputing Resource Center.

5. REFERENCES

1. Thostenson, Erik T., Zhifeng Ren, and Tsu-Wei Chou. "Advances in the science and technology of carbon nanotubes and their composites: a review." *Composites science and technology* 61, no. 13 (2001): 1899-1912. https://doi.org/10.1016/S0266-3538(01)00094-X
2. Datta, Siddhant, Masoud Yekani Fard, and Aditi Chattopadhyay. "High-speed surfactant-free fabrication of large carbon nanotube membranes for multifunctional composites." *Journal of Aerospace Engineering* 29, no. 3 (2015): 04015060. https://doi.org/10.1061/(ASCE)AS.1943-5525.0000558
3. Datta, Siddhant, Rajesh Kumar Neerukatti, and Aditi Chattopadhyay. "Buckypaper Embedded Self-Sensing Composite for Real-Time Fatigue Damage Diagnosis and Prognosis." *Carbon* (2018). https://doi.org/10.1016/j.carbon.2018.06.059
4. Rai, Ashwin, Siddhant Datta, Aditi Chattopadhyay, and Carlos Lopez. "Reinforcement of Composite Joint Interface Using Nanomaterials." In *ASME 2017 International Mechanical Engineering Congress and Exposition*, pp. V009T12A002-V009T12A002. American Society of Mechanical Engineers, 2017. http://doi.org10.1115/IMECE2017-72623.
5. Green, Keith J., Derrick R. Dean, Uday K. Vaidya, and Elijah Nyairo. "Multiscale fiber reinforced composites based on a carbon nanofiber/epoxy nanophased polymer matrix: synthesis, mechanical, and thermomechanical behavior." *Composites Part A: applied science and manufacturing* 40, no. 9(2009):1470-1475. https://doi.org/10.1016/j.compositesa.2009.05.010
6. Seyhan, A. Tugrul, Metin Tanoglu, and Karl Schulte. "Mode I and mode II fracture toughness of E-glass non-crimp fabric/carbon nanotube (CNT) modified polymer-based composites." *Engineering Fracture Mechanics* 75, no. 18 (2008): 5151-5162. https://doi.org/10.1016/j.engfracmech.2008.08.003
7. Thakre, Piyush R., Dimitris C. Lagoudas, Jaret C. Riddick, Thomas S. Gates, Sarah-Jane V. Frankland, James G. Ratcliffe, Jiang Zhu, and Enrique V. Barrera. "Investigation of the effect of single wall carbon nanotubes on interlaminar fracture toughness of woven carbon fiber—epoxy composites." *Journal of Composite Materials* 45, no. 10 (2011): 1091-1107. https://doi.org/10.1177/0021998310389088
8. Godara, Ajay, L. Mezzo, F. Luizi, A. Warrier, Stepan Vladimirovitch Lomov, A. W. Van Vuure, L. Gorbatikh, P. Moldenaers, and I. Verpoest. "Influence of carbon nanotube reinforcement on the processing and the mechanical behaviour of carbon fiber/epoxy composites." *Carbon* 47, no. 12 (2009): 2914-2923. https://doi.org/10.1016/j.carbon.2009.06.039
9. Chou, Tsu-Wei, Limin Gao, Erik T. Thostenson, Zuoguang Zhang, and Joon-Hyung Byun. "An assessment of the science and technology of carbon nanotube-based fibers and composites." *Composites Science and Technology* 70, no. 1 (2010): 1-19. https://doi.org/10.1016/j.compscitech.2009.10.004
10. Sharma, S. P., and S. C. Lakkad. "Effect of CNTs growth on carbon fibers on the tensile strength of CNTs grown carbon fiber-reinforced polymer matrix composites." *Composites Part A: Applied Science and Manufacturing* 42, no. 1 (2011): 8-15. https://doi.org/10.1016/j.compositesa.2010.09.008

11. Wicks, Sunny S., Roberto Guzman de Villoria, and Brian L. Wardle. "Interlaminar and intralaminar reinforcement of composite laminates with aligned carbon nanotubes." *Composites Science and Technology* 70, no. 1 (2010): 20-28. https://doi.org/10.1016/j.compscitech.2009.09.001

12. Carpenter, C. R., P. H. Shipway, Y. Zhu, and D. P. Weston. "Effective dispersal of CNTs in the fabrication of electrodeposited nanocomposites." *Surface and Coatings Technology* 205, no. 20 (2011): 4832-4837. https://doi.org/10.1016/j.surfcoat.2011.04.070

13. Qian H, Bismarck A, Greenhalgh ES, Kalinka G, Shaffer MSP. Hierarchical composites reinforced with carbon nanotube grafted fibers: the potential assessed at the single fiber level. Chem Mater 2008; 20(5): 1862–9. https://doi.org/ 10.1021/cm702782j

14. Wang C, Li Y, Tong L, Song Q, Li K, Li J, et al. The role of grafting force and surface wettability in interfacial enhancement of carbon nanotube/carbon fiber hierarchical composites. Carbon 9 (2014) 239–46. https://doi.org/10.1016/j.carbon.2013.12.020

15. Huang, Sheng-Yun, Gang-Ping Wu, Cheng-Meng Chen, Yu Yang, Shou-Chun Zhang, and Chun-Xiang Lu. "Electrophoretic deposition and thermal annealing of a graphene oxide thin film on carbon fiber surfaces." *Carbon* 52 (2013): 613-616. https://doi.org/10.1016/j.carbon.2012.09.062

16. Karapappas, P., A. Vavouliotis, P. Tsotra, V. Kostopoulos, and A. Paipetis. "Enhanced fracture properties of carbon reinforced composites by the addition of multi-wall carbon nanotubes." *Journal of Composite Materials* 43, no. 9 (2009): 977-985. https://doi.org/10.1177/0021998308097735

17. Garcia, Enrique J., Brian L. Wardle, and A. John Hart. "Joining prepreg composite interfaces with aligned carbon nanotubes." *Composites Part A: Applied Science and Manufacturing* 39, no. 6 (2008): 1065-1070. https://doi.org/10.1016/j.compositesa.2008.03.011

18. Wood, Charles D., Marc J. Palmeri, Karl W. Putz, Gregory Ho, Rick Barto, and L. Catherine Brinson. "Nanoscale structure and local mechanical properties of fiber-reinforced composites containing MWCNT-grafted hybrid glass fibers." *Composites Science and Technology* 72, no. 14 (2012): 1705-1710. https://doi.org/10.1016/j.compscitech.2012.06.008

19. Chatzigeorgiou, George, Yalchin Efendiev, and Dimitris C. Lagoudas. "Homogenization of aligned “fuzzy fiber” composites." *International Journal of Solids and Structures* 48, no. 19 (2011): 2668-2680. https://doi.org/10.1016/j.ijsolstr.2011.05.011

20. Chatzigeorgiou, George, Gary Don Seidel, and Dimitris C. Lagoudas. "Effective mechanical properties of “fuzzy fiber” composites." *Composites Part B: Engineering* 43, no. 6 (2012): 2577-2593. https://doi.org/10.1016/j.compositesb.2012.03.001

21. Kundalwal, S. I., and M. C. Ray. "Effective properties of a novel continuous fuzzy-fiber reinforced composite using the method of cells and the finite element method." *European Journal of Mechanics-A/Solids* 36 (2012): 191-203. https://doi.org/10.1016/j.euromechsol.2012.03.006

22. Rafiee, Roham, and Amin Ghorbanhosseini. "Predicting mechanical properties of fuzzy fiber reinforced composites: radially grown carbon nanotubes on the carbon fiber." *International Journal of Mechanics and Materials in Design*: 1-14. https://doi.org/10.1007/s10999-016-9359-9

23. Wicks, Sunny S., Wennie Wang, Marcel R. Williams, and Brian L. Wardle. "Multi-scale interlaminar fracture mechanisms in woven composite laminates reinforced with aligned carbon nanotubes." *Composites Science and Technology* 100 (2014): 128-135. https://doi.org/10.1016/j.compscitech.2014.06.003

24. Koo, B., Liu, Y., Zou, J., "Study of glass transition temperature (Tg) of novel stress-sensitive composites using molecular dynamic simulation," *Modelling and Simulation in Materials Science and Engineering,* Vol. 22, No. 6, 2014, pp. 065018. http://dx.doi.org/10.1088/0965-0393/22/6/065018

25. Subramanian, Nithya, Ashwin Rai, and Aditi Chattopadhyay. "Atomistically informed stochastic multiscale model to predict the behavior of carbon nanotube-enhanced nanocomposites." *Carbon* 94 (2015): 661-672. https://doi.org/10.1016/j.carbon.2015.07.051

26. Subramanian, Nithya, Bonsung Koo, Karthik Rajan Venkatesan, and Aditi Chattopadhyay. "Computational analysis for the interface mechanics of carbon fibers with radially-grown carbon nanotubes." *Carbon* 134 (2018): 123-133. https://doi.org/10.1016/j.carbon.2018.03.090

27. Rai, A., Subramanian, N., Koo, B., Chattopadhyay, A., 2016. Multiscale damage analysis of cnt nanocomposite using a continuum damage mechanics approach. J. Compos. Mater. https://doi.org/10.1177%2F0021998316654304

28. Venkatesan, Karthik Rajan, Nithya Subramanian, Ashwin Rai, and Aditi Chattopadhyay. "Atomistically informed multiscale modeling of radially grown nanocomposite using a continuum damage mechanics approach." *Carbon* 142 (2019): 420-429. https://doi.org/10.1016/j.carbon.2018.10.051

29. ASTM. "Standard guide for use of adhesive-bonded single lap-joint specimen test results." *ASTM D 4896-95* (1995).

30. Berry, J. P. "Some kinetic considerations of the Griffith criterion for fracture—I: Equations of motion at constant force." *Journal of the Mechanics and Physics of Solids* 8, no. 3 (1960): 194-206. https://doi.org/10.1016/0022-5096(60)90038-7